*Appl. Math. Mech. -Engl. Ed.*, **42**(3), 357–370 (2021)

**APPLIED MATHEMATICS AND MECHANICS (ENGLISH EDITION)**

https://doi.org/10.1007/s10483-021-2700-7

# Stability analysis and modeling for the three-dimensional Darcy-Forchheimer stagnation point nanofluid flow towards a moving surface*

Yuming CHU[1,2], M. I. KHAN[3,†], M. I. U. REHMAN[4], S. KADRY[5], S. QAYYUM[4], M. WAQAS[6]

1. Department of Mathematics, Huzhou University, Huzhou 313000, Zhejiang Province, China;
2. Hunan Provincial Key Laboratory of Mathematical Modeling and Analysis in Engineering, Changsha University of Science & Technology, Changsha 410114, China;
3. Department of Mathematics, Riphah International University, Faisalabad Campus, Faisalabad 38000, Pakistan;
4. Department of Mathematics, Quaid-i-Azam University, Islamabad 44000, Pakistan;
5. Department of Mathematics and Computer Science, Beirut Arab University, Beirut 11072809, Lebanon;
6. NUTECH School of Applied Sciences and Humanities, National University of Technology, Islamabad 44000, Pakistan

(Received Aug. 15, 2020 / Revised Nov. 20, 2020)

**Abstract** In this research, the three-dimensional (3D) steady and incompressible laminar Homann stagnation point nanofluid flow over a porous moving surface is addressed. The disturbance in the porous medium has been characterized by the Darcy-Forchheimer relation. The slip for viscous fluid is considered. The energy equation is organized in view of radiative heat flux which plays an important role in the heat transfer rate. The governing flow expressions are first altered into first-order ordinary ones and then solved numerically by the shooting method. Dual solutions are obtained for the velocity, skin friction coefficient, temperature, and Nusselt number subject to sundry flow parameters, magnetic parameter, Darcy-Forchheimer number, thermal radiation parameter, suction parameter, and dimensionless slip parameter. In this research, the main consideration is given to the engineering interest like skin friction coefficient (velocity gradient or surface drag force) and Nusselt number (temperature gradient or heat transfer rate) and discussed numerically through tables. In conclusion, it is noticed from the stability results that the upper branch solution (UBS) is more reliable and physically stable than the lower branch solution (LBS).

* Citation: CHU, Y. M., KHAN, M. I., REHMAN, M. I. U., KADRY, S., QAYYUM, S., and WAQAS, M. Stability analysis and modeling for the three-dimensional Darcy-Forchheimer stagnation point nanofluid flow towards a moving surface. *Applied Mathematics and Mechanics* (*English Edition*), **42**(3), 357–370 (2021) https://doi.org/10.1007/s10483-021-2700-7

† Corresponding author, E-mail: mikhan@math.qau.edu.pk

Project supported by the National Natural Science Foundation of China (Nos. 11971142, 11871202, 61673169, 11701176, 11626101, and 11601485)

**Key words** viscous slip, Darcy-Forchheimer relation, thermal radiation, stagnation point flow, dual solution, heat generation/absorption, stability result

**Chinese Library Classification** O361
**2010 Mathematics Subject Classification** 76A05, 76A10, 76Rxx, 76Wxx

**Nomenclature**

| | |
|---|---|
| $\xi U$, $\xi V$, | velocities in $x$- and $y$-directions, respectively; |
| $\alpha$, | momentum accommodation coefficient; |
| $K^*$, | permeability of porous space; |
| $Kn$, | Knudsen number; |
| $\Lambda$, | mean free path; |
| $M_1$,$M_2$, | slip coefficients in $x$- and $y$-directions; |
| $x$, $y$, $z$, | Cartesian coordinates; |
| $u$, $v$, $w$, | velocity vectors; |
| $T_\infty$, | ambient temperature; |
| $k^*$, | mean absorption coefficient; |
| $Q^*$, | heat generation/absorption coefficient; |
| $\beta^*$, | porosity parameter; |
| $Re$, | Reynold number; |
| $C_{f1}, C_{f2}$, | skin frictions; |
| $Nu$, | Nusselt number; |
| $\nu_{\rm nf}$, | kinematic viscosity; |
| $F\big(\frac{C_b}{xK^{*\frac{1}{2}}}\big)$, | coefficient of non-uniform inertia; |
| $T$, | temperature; |
| $c_p$, | specific heat; |
| $k_{\rm nf}$, | thermal conductivity; |
| $\sigma^*$, | Stefan-Boltzmann constant; |
| $u_w(x)$, | stretching velocity; |
| $C_b$, | drag coefficient; |
| $\mu_{\rm f}$, | dynamic viscosity; |
| $w_0$, | suction/injection; |
| $T_{\rm w}$, | wall temperature; |
| $s$, | suction/injection variable; |
| $Pr$, | Prandtl number; |
| $R$, | radiation number; |
| $A, B$, | slip parameters in $x$- and $y$-directions; |
| $\lambda, \lambda_1$, | dimensionless constant parameters; |
| $Q^*$, | heat generation parameter; |
| $F_x, F_y$, | coefficients of inertia in $x$- and $y$-directions. |

## 1 Introduction

The concept of boundary layer flows is acknowledged in various fields of applied mathematics, mechanical and electrical engineering, physics and biomedical and chemical engineering applications, for example, wires, manufacturing of plastics films, liquid films in concentration process, crystal growth, continuous filament extrusion from a peroxide, pharmaceutical industries, windup roll, cooling of an inestimable metallic plate in a cooling bath and so on. The heat transport has played an important role in the above processes. The rate of cooling convinces extraordinary towards the superiority of final items with favored attributes. In addition, the mass transmission is used in various frameworks and techniques that engage he convective and molecular transport of molecules and atoms. For example, the mass transport is included in dehydration. The boundary layer flow has gained much attention by linearly stretched and flat surface of numerous researchers and analysts in the last few couples of years, which are regarded in Refs. [1]–[5]. These research studies investigate the different physical characteristic behaviors on the heat transport and liquid flow. Also, the fluid flow with the boundary layer concept stimulated by a stretched surface encloses the glass fiber, extrusion process, electronic chips, paper production, crystal growing, and many therein. In 1961, Sakiadis[6] utilized the concept of boundary layer in axisymmetric flow on continuous sloid surfaces. After, Crane[7] investigated the fluid flow behavior over a stretchable and flat surface. Heat and mass transport in electrically conducting flow of viscoelastic material by a vertical stretched surface with thermo diffusion (Soret and Dufour) effects were scrutinized by Rashidi et al.[8]. The bibliography on such fruitful and significant flows is moderately massive, and some research attempts in this direction can be seen in Refs. [9]–[11]. These communications analyzed the impact of viscous dissipation and heat source/sink, and it is publicized that both phenomena considerably affect the heat transport rate by augmenting it.

The investigation of stagnation point flows has fascinated the concentration of frequent analysts and engineers due to its meaningful and considerable applications in industrial and

mechanical engineering processes. The stagnation point flow is categorized in two types, namely, axisymmetric and plane stagnation point flows. The laminar flow towards a plane stagnation point flow was also referred as Hiemenz flow and initially investigated by Schlichting[12]. Behaviors of particle depositions in such kind of framework were explored by Chari and Rajagopalan[13]. On the other hand, the axisymmetric flow near stagnation point is also referred as symmetrical radial or impinging jet stagnation flow is analogous in various aspects to the former framework. In this paper, we will deal with the fluid flow subject to various flow assumptions and aspects near stagnation point and such fruitful and interesting research articles are mentioned in Refs. [14]–[20].

This communication interprets the salient characteristics of first-order velocity for three-dimensional (3D), steady, incompressible, Darcy-Forchheimer Homann stagnation point nanofluid flow by a moving surface. Also, this work was the extension of Hafidzuddin et al.[14] with Darcy-Forchheimer porous relation, thermal radiation, and heat generation/absorption effects. The flow is generated by slip effect and stretching phenomenon, and saturated through Darcy-Forchheimer relation. The energy equation is organized in the presence of heat generation/absorption and thermal radiation effect, where these effects play an important role in the transportation of heat. Dual solutions for the present problem are obtained through the shooting method (bvp4c). The engineering interests like skin friction and Nusselt number are calculated numerically in the presence of important flow parameter, and displayed in the tabular form.

## 2 Coordinate system and modeling

In this research work, the mathematical modeling is developed for the incompressible, steady, 3D nanofluid flow of viscous material past a moving porous surface with Darcy-Forchheimer relation and first-order velocity slip. The velocity slip occurs when there is difference between the velocity of sheet and the adjacent particles which are attached to the sheet. The thermal radiation occurs when all the particles are heated and starts releasing kinetic energy due to which particles start vibrating. Such energy formed by this vibration of particles is called thermal radiation. In the present flow system, we have taken thermal radiation in the flow direction along the $z$-axis. The heat source effect is used in the thermal equation to increase the temperature of the fluid. The flow problem is discussed in semi-infinite domain of Cartesian coordinates, i.e., in the $xy$-plane with $x$- and $y$-axes aligned along and normal to the striation on the porous plate. The fluid is placed along the $z$-axis. Let the plate move out or inside the center with velocities $\xi U$ and $\xi V$ respectively in the $x$- and $y$-directions. The dimensionless moving parameter is positive ($\xi > 0$) when the plate moves away the origin and is negative ($\xi < 0$) when the plate moves inside the origin. Figure 1 illustrates for the schematic flow analysis. The boundary condition $v = w_0$ indicates the mass flux velocity. There are two cases for mass flux velocity (i) ($w_0 > 0$) suction and (ii) ($w_0 < 0$) injection or known as blowing. Furthermore, the outer velocities are represented by $u_e(x) = ax$, $v_e(y) = ay$, and $w_e(x) = -2az$. In view of above assumptions, the governing equations for viscous fluid can be addressed as follows[14]:

$$\frac{\partial u}{\partial x} + \frac{\partial v}{\partial y} + \frac{\partial w}{\partial z} = 0, \tag{1}$$

$$u\frac{\partial u}{\partial x} + v\frac{\partial u}{\partial y} + w\frac{\partial w}{\partial z} = u_e\frac{\partial u_e}{\partial x} + \nu_{\rm nf}\nabla^2 u - \frac{\nu_{\rm nf}}{K^*}(u - u_e) - F(u^2 - u_e^2), \tag{2}$$

$$u\frac{\partial v}{\partial x} + v\frac{\partial v}{\partial y} + w\frac{\partial v}{\partial z} = v_e\frac{\partial v_e}{\partial x} + \nu_{\rm nf}\nabla^2 v - \frac{\nu_{\rm nf}}{K^*}(v - v_e) - F(v^2 - v_e^2), \tag{3}$$

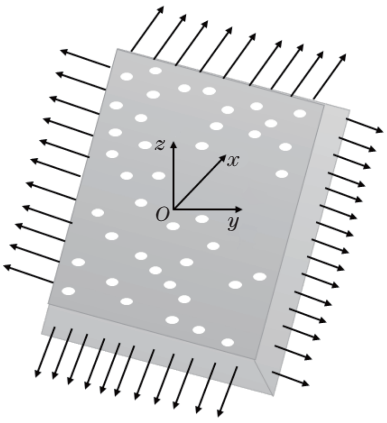


**Fig. 1** Flow geometry

$$u\frac{\partial w}{\partial x}+v\frac{\partial w}{\partial y}+w\frac{\partial w}{\partial z}=w_e\frac{\partial w_e}{\partial x}+\nu_{\rm nf}\nabla^2 w-\frac{\nu_{\rm nf}}{K^*}(w-w_e)-F(w^2-w_e^2), \tag{4}$$

$$u\frac{\partial T}{\partial x}+v\frac{\partial T}{\partial y}+w\frac{\partial T}{\partial z}=\frac{1}{(\rho c_p)_{\rm nf}}\Big(k_{\rm nf}+\frac{16\sigma^* T_\infty^3}{3k^*}\Big)\nabla^2 T+\frac{Q^*}{(\rho c_p)_{\rm nf}}(T-T_\infty) \tag{5}$$

with

$$\begin{cases} u=u_w(x)=\xi U+U_{\rm slip}, \quad v=v_w(y)=\xi V+V_{\rm slip}, \quad w=w_0, \quad T=T_{\rm w} \quad \text{at} \quad z=0,\\ u=u_e(x)\to ax, \quad v=v_e(y)\to ay, \quad w=w_e(z)\to -2az, \quad T\to T_\infty \quad \text{as} \quad z\to\infty, \end{cases} \tag{6}$$

where $U_{\rm slip}$ and $V_{\rm slip}$ are defined as

$$\begin{cases} U_{\rm slip}=\dfrac{2}{3}\Big(\dfrac{3-\alpha l^3}{\alpha}-\dfrac{3}{2}\dfrac{1-l^2}{Kn}\Big)\Lambda\dfrac{\partial u}{\partial z}, \quad V_{\rm slip}=\dfrac{2}{3}\Big(\dfrac{3-\alpha l^3}{\alpha}-\dfrac{3}{2}\dfrac{1-l^2}{Kn}\Big)\Lambda\dfrac{\partial v}{\partial z},\\ U_{\rm slip}=M_1\dfrac{\partial u}{\partial z}, \quad V_{\rm slip}=M_2\dfrac{\partial v}{\partial z}, \end{cases}$$

in which $\alpha$, $l$, $Kn$, and $\Lambda$ are defined as momentum accommodation coefficient with $0\leqslant\alpha\leqslant 1$, $l=\min[1/Kn,1]$, $Kn$ is the Knudsen number defined as mean free path $\Lambda$ divided by a characteristic length for the flow, and $\Lambda$ is molecular mean free path. For any value of $Kn$, $l$ is always between 0 to 1. Also we know that $\Lambda$ is always positive. So from all the above values we conclude that $M_1$ and $M_2$ are positive. In the above governing expressions, $x$, $y$, and $z$ indicate the Cartesian coordinates, $u$, $v$, and $w$ indicate the velocity components, $u_e$ indicates the free stream velocity, $\nabla$ indicates the operator, $\nu_{\rm nf}$ indicates the kinematic viscosity, $K^*$ indicates the permeability of porous space, $F\big(\frac{C_b}{xK^{*\frac{1}{2}}}\big)$ indicates the coefficient of non-uniform inertia, $T$ indicates the temperature, $c_p$ indicates the specific heat, $k_{\rm nf}$ indicates the thermal conductivity, $\sigma^*$ indicates the Stefan-Boltzmann constant, $T_\infty$ indicates the ambient temperature, $k^*$ indicates the mean absorption coefficient, $Q^*$ indicates the heat generation/absorption coefficient, $u_w(x)$ indicates the stretching velocity, $M_1$, $M_2$ indicate the constant slip coefficients, $C_b$ indicates the drag coefficient, $\mu_{\rm f}$ indicates the dynamic viscosity, $w_0$ indicates the suction/injection, $T_{\rm w}$ indicates the wall temperature, and $a$ indicates the positive dimensional constant. Note that $z=0$ indicates the plate surface.

Now we have used transformations which are usually utilized for 3D steady incompressible flow. These transformations are drawn from Blasius equation-first-order boundary layer. There is little modification in these transformations from basic Blasius equation-first-order boundary

layer due to the reason that plate moves out or inside the center with velocities $\xi U$ and $\xi V$ respectively in the $x$- and $y$-directions. We have also considered slip condition, thermal radiation, Darcy effect, heat generation effect, and stagnation point flow. For these type of assumption transformations mentioned below are perfect. Consider the following equations[13]:

$$\begin{cases} u = axf'(\eta) + Uh(\eta), \quad v = ayg'(\eta) + Vk(\eta), \quad w = -\sqrt{a\nu_{\rm f}}(f(\eta) + g(\eta)), \\ \eta = \sqrt{\dfrac{a}{\nu_{\rm f}}}z, \quad \theta = \dfrac{T - T_\infty}{T_{\rm w} - T_\infty}. \end{cases} \tag{7}$$

In Eq. (7), primes highlight the differentiation subject to $\eta$. On the plate surface the normal component of velocity is $w_0$, therefore, $f(0) + g(0) = s$, where $s = -\sqrt{a\nu_{\rm f}}$ signifies the surface mass transport variable. There are two cases: (i) $s > 0$ suction; (ii) $s < 0$ injection. Without loss of generality, we arrive $f(0) = s$ and $g(0) = 0$.

**Table 1** Transport characteristics of nanomaterials

| Property | Nanomaterial |
|---|---|
| Density | $\rho_{\rm nf} = \rho_{\rm f}\big(1 - \varphi + \varphi\frac{\rho_{\rm s}}{\rho_{\rm f}}\big)$ |
| Viscosity | $\mu_{\rm nf} = \frac{\mu_{\rm f}}{(1-\varphi)^{2.5}}$ |
| Heat capacity | $(\rho c_p)_{\rm nf} = (\rho c_p)_{\rm f}\big(1 - \varphi + \varphi\frac{(\rho c_p)_{\rm s}}{(\rho c_p)_{\rm f}}\big)$ |
| Thermal conductivity | $\frac{k_{\rm nf}}{k_{\rm f}} = \frac{k_{\rm s}+2k_{\rm f}-2\varphi(k_{\rm f}-k_{\rm s})}{k_{\rm s}+2k_{\rm f}+2\varphi(k_{\rm f}-k_{\rm s})}$ |

After implementing the transformations, we obtain

$$\Big(\frac{\mu_{\rm nf}}{\mu_{\rm f}}\Big)\Big(\frac{\rho_{\rm f}}{\rho_{\rm nf}}\Big)f''' + (f+g)f'' - f'^2 + 1 - \beta^*\Big(\frac{\mu_{\rm nf}}{\mu_{\rm f}}\Big)\Big(\frac{\rho_{\rm f}}{\rho_{\rm nf}}\Big)(f'-1) - F_x(f'^2-1) = 0, \tag{8}$$

$$\Big(\frac{\mu_{\rm nf}}{\mu_{\rm f}}\Big)\Big(\frac{\rho_{\rm f}}{\rho_{\rm nf}}\Big)g''' + (f+g)g'' - g'^2 + 1 - \beta^*\Big(\frac{\mu_{\rm nf}}{\mu_{\rm f}}\Big)\Big(\frac{\rho_{\rm f}}{\rho_{\rm nf}}\Big)(g'-1) - F_y(g'^2-1) = 0, \tag{9}$$

$$\Big(\frac{\mu_{\rm nf}}{\mu_{\rm f}}\Big)\Big(\frac{\rho_{\rm f}}{\rho_{\rm nf}}\Big)h'' + (f+g)h' - hf' - \beta^*\Big(\frac{\mu_{\rm nf}}{\mu_{\rm f}}\Big)\Big(\frac{\rho_{\rm f}}{\rho_{\rm nf}}\Big)(h) - F_x(\lambda h^2 + 2hf') = 0, \tag{10}$$

$$\Big(\frac{\mu_{\rm nf}}{\mu_{\rm f}}\Big)\Big(\frac{\rho_{\rm f}}{\rho_{\rm nf}}\Big)k'' + (f+g)k' - kg' - \beta^*\Big(\frac{\mu_{\rm nf}}{\mu_{\rm f}}\Big)\Big(\frac{\rho_{\rm f}}{\rho_{\rm nf}}\Big)(k) - F_y(\lambda_1 k^2 + 2kf') = 0, \tag{11}$$

$$\Big(\frac{1}{Pr}\Big)\Big(\frac{(\rho c_p)_{\rm f}}{(\rho c_p)_{\rm nf}}\Big)\Big(\Big(\frac{k_{\rm nf}}{k_{\rm f}} + R\Big)\Big)\theta'' + (f+g)\theta' + Q\Big(\frac{(\rho c_p)_{\rm f}}{(\rho c_p)_{\rm nf}}\Big)\theta = 0 \tag{12}$$

with

$$\begin{cases} f(0) = s, \quad g(0) = 0, \\ f'(0) = Af''(0), \quad g'(0) = Bg''(0), \\ h(0) = Ah'(0) + \xi, \quad k(0) = Bk'(0) + \xi, \\ f'(\infty) \to 1, \quad g'(\infty) \to 1, \quad h(\infty) \to 0, \quad k(\infty) \to 0. \end{cases} \tag{13}$$

Note that, $Pr\,\big(= \frac{(\rho c_p)_{\rm f}\nu_{\rm f}}{k_{\rm f}}\big)$ indicates the Prandtl number, $A\,\big(= M_1\sqrt{\frac{a}{\nu_{\rm f}}}\big)$ and $B\,\big(= M_2\sqrt{\frac{a}{\nu_{\rm f}}}\big)$ indicate the slip parameters in $x$- and $y$-directions, $s\,\big(= \frac{-w_0}{\sqrt{a\nu_{\rm f}}}\big)$ indicates the suction/injection parameter, $R\,\big(= \frac{16\sigma^* T_\infty^3}{3k_{\rm f}k^*}\big)$ indicates the radiation parameter, $\lambda\,\big(= \frac{U}{ax}\big)$ and $\lambda_1\big(= \frac{V}{ay}\big)$ indicate the dimensionless constants, $\beta^*\,\big(= \frac{\nu_{\rm f}}{K^* a}\big)$ indicates the porosity parameter, $Q\,\big(= \frac{Q^*}{a(\rho c_p)_{\rm f}}\big)$ indicates the heat generation/absorption parameter, $Re = \frac{U_w x}{\nu_{\rm f}}$ indicates the Reynolds number, and $F_x = Fx$ and $F_y = Fy$ indicate the coefficients of the inertia porous medium.

The physical quantities or engineering interest like the skin friction ($C_f$) and the Nusselt number or the temperature gradient ($Nu$) are defined as

$$\begin{cases} C_{f1} = \dfrac{\tau_{zx}}{\rho_{\mathrm{f}}(ax)^2}, \\ C_{f2} = \dfrac{\tau_{zy}}{\rho_{\mathrm{f}}(ay)^2}, \end{cases} \tag{14}$$

$$Nu = \frac{xq_{\mathrm{w}}}{k_{\mathrm{f}}(T - T_\infty)}, \tag{15}$$

where $\tau_{zx}$, $\tau_{zy}$, and $q_{\mathrm{w}}$ indicate the shear stresses and heat flux,

$$\begin{cases} \tau_{zx} = \mu_{\mathrm{nf}}\Big(\dfrac{\partial u}{\partial z}\Big), \\ \tau_{zy} = \mu_{\mathrm{nf}}\Big(\dfrac{\partial v}{\partial z}\Big). \end{cases} \tag{16}$$

$$q_{\mathrm{w}} = -k_{\mathrm{nf}}\frac{\partial T}{\partial z}\Big|_{z=0} + O_{\mathrm{T}}, \tag{17}$$

in which $O_{\mathrm{T}}$ indicates the thermal radiation term. Finally, one has

$$\begin{cases} C_{f1}Re^{0.5} = \dfrac{\mu_{\mathrm{nf}}}{\mu_{\mathrm{f}}}k'(0), \\ C_{f2}Re^{0.5} = \dfrac{\mu_{\mathrm{nf}}}{\mu_{\mathrm{f}}}f''(0), \end{cases} \tag{18}$$

$$NuRe^{-0.5} = -\theta'(0). \tag{19}$$

## 3 Stability study

In this section, we checked the dual solutions, i.e., the UBS and the LBS, are stable or unstable of the flow expressions (8)–(12) through stability study. To start the stability study, we consider the time dependent state of boundary value problem (1)–(5). Equation (1) automatically holds and the remaining equations take the following form:

$$\frac{\partial u}{\partial t} + u\frac{\partial u}{\partial x} + v\frac{\partial u}{\partial y} + w\frac{\partial w}{\partial z} = u_e\frac{\partial u_e}{\partial x} + \nu_{\mathrm{nf}}\nabla^2 u - \frac{\nu_{\mathrm{nf}}}{K^*}(u - u_e) - F(u^2 - u_e^2), \tag{20}$$

$$\frac{\partial v}{\partial t} + u\frac{\partial v}{\partial x} + v\frac{\partial v}{\partial y} + w\frac{\partial v}{\partial z} = v_e\frac{\partial v_e}{\partial x} + \nu_{\mathrm{nf}}\nabla^2 v - \frac{\nu_{\mathrm{nf}}}{K^*}(v - v_e) - F(v^2 - v_e^2), \tag{21}$$

$$\frac{\partial w}{\partial t} + u\frac{\partial w}{\partial x} + v\frac{\partial w}{\partial y} + w\frac{\partial w}{\partial z} = w_e\frac{\partial w_e}{\partial x} + \nu_{\mathrm{nf}}\nabla^2 w - \frac{\nu_{\mathrm{nf}}}{K^*}(w - w_e) - F(w^2 - w_e^2), \tag{22}$$

$$\frac{\partial T}{\partial t} + u\frac{\partial T}{\partial x} + v\frac{\partial T}{\partial y} + w\frac{\partial T}{\partial z} = \frac{1}{(\rho c_p)_{\mathrm{nf}}}\Big(k_{\mathrm{nf}} + \frac{16\sigma^* T_\infty^3}{3k^*}\Big)\nabla^2 T + \frac{Q^*}{(\rho c_p)_{\mathrm{nf}}}(T - T_\infty). \tag{23}$$

Here, we introduce a new time dependent dimensionless variable[22], i.e., $\tau = at$. The utilization of new time dependent dimensionless variable which is associated with IVP and is reliable with the question of which solution will be achieved in physically realizable. Now we have

$$\begin{cases} u = ax\dfrac{\partial f}{\partial \eta}(\eta, \tau) + Uh(\eta, \tau), \quad v = ay\dfrac{\partial g}{\partial \eta}(\eta, \tau) + Vk(\eta, \tau), \\ w = -\sqrt{a\nu_{\mathrm{f}}}(f(\eta, \tau) + g(\eta, \tau)), \quad \eta = \sqrt{\dfrac{a}{\nu_{\mathrm{f}}}}z, \quad \theta(\eta, \tau) = \dfrac{T - T_\infty}{T_{\mathrm{w}} - T_\infty}, \quad \tau = at. \end{cases} \tag{24}$$

Then, Eqs. (20)–(23) are addressed as

$$\Big(\frac{\mu_{\rm nf}}{\mu_{\rm f}}\Big)\Big(\frac{\rho_{\rm f}}{\rho_{\rm nf}}\Big)\frac{\partial^3 f}{\partial\eta^3}+(f+g)\frac{\partial^2 f}{\partial\eta^2}-\frac{\partial^2 f}{\partial\eta^2}+1-\beta^*\Big(\frac{\mu_{\rm nf}}{\mu_{\rm f}}\Big)\Big(\frac{\rho_{\rm f}}{\rho_{\rm nf}}\Big)\Big(\frac{\partial f}{\partial\eta}-1\Big)$$
$$-F_x\Big(\frac{\partial^2 f}{\partial\eta^2}-1\Big)-\frac{\partial^2 f}{\partial\eta\partial\tau}=0, \tag{25}$$

$$\Big(\frac{\mu_{\rm nf}}{\mu_{\rm f}}\Big)\Big(\frac{\rho_{\rm f}}{\rho_{\rm nf}}\Big)\frac{\partial^3 g}{\partial\eta^3}+(f+g)\frac{\partial^2 g}{\partial\eta^2}-\frac{\partial^2 g}{\partial\eta^2}+1-\beta^*\Big(\frac{\mu_{\rm nf}}{\mu_{\rm f}}\Big)\Big(\frac{\rho_{\rm f}}{\rho_{\rm nf}}\Big)\Big(\frac{\partial g}{\partial\eta}-1\Big)$$
$$-F_y\Big(\frac{\partial^2 g}{\partial\eta^2}-1\Big)-\frac{\partial^2 g}{\partial\eta\partial\tau}=0, \tag{26}$$

$$\Big(\frac{\mu_{\rm nf}}{\mu_{\rm f}}\Big)\Big(\frac{\rho_{\rm f}}{\rho_{\rm nf}}\Big)\frac{\partial^2 h}{\partial\eta^2}+(f+g)\frac{\partial h}{\partial\eta}-h\frac{\partial f}{\partial\eta}-\beta^*\Big(\frac{\mu_{\rm nf}}{\mu_{\rm f}}\Big)\Big(\frac{\rho_{\rm f}}{\rho_{\rm nf}}\Big)(h)$$
$$-F_x\Big(\lambda\frac{\partial^2 h}{\partial\eta^2}+2h\frac{\partial f}{\partial\eta}\Big)-\frac{\partial h}{\partial\tau}=0, \tag{27}$$

$$\Big(\frac{\mu_{\rm nf}}{\mu_{\rm f}}\Big)\Big(\frac{\rho_{\rm f}}{\rho_{\rm nf}}\Big)\frac{\partial^2 k}{\partial\eta^2}+(f+g)\frac{\partial k}{\partial\eta}-k\frac{\partial g}{\partial\eta}-\beta^*\Big(\frac{\mu_{\rm nf}}{\mu_{\rm f}}\Big)\Big(\frac{\rho_{\rm f}}{\rho_{\rm nf}}\Big)(k)$$
$$-F_y\Big(\lambda_1\frac{\partial^2 k}{\partial\eta^2}+2k\frac{\partial f}{\partial\eta}\Big)-\frac{\partial h}{\partial\tau}=0, \tag{28}$$

$$\Big(\frac{1}{Pr}\Big)\Big(\frac{(\rho c_p)_{\rm f}}{(\rho c_p)_{\rm nf}}\Big)\Big(\Big(\frac{k_{\rm nf}}{k_{\rm f}}+R\Big)\Big)\frac{\partial^2\theta}{\partial\eta^2}+(f+g)\frac{\partial\theta}{\partial\eta}+Q\Big(\frac{(\rho c_p)_{\rm f}}{(\rho c_p)_{\rm nf}}\Big)\theta=0 \tag{29}$$

with

$$\begin{cases} f(0,\tau)=s,\quad g(0,\tau)=0,\quad \dfrac{\partial f}{\partial\eta}(0,\tau)=A\dfrac{\partial^2 f}{\partial\eta^2}(0,\tau),\quad \dfrac{\partial g}{\partial\eta}(0,\tau)=B\dfrac{\partial^2 g}{\partial\eta^2}(0,\tau),\\ h(0,\tau)=A\dfrac{\partial h}{\partial\eta}(0,\tau)+\xi,\quad k(0,\tau)=B\dfrac{\partial k}{\partial\eta}(0,\tau)+\xi,\\ \dfrac{\partial f}{\partial\eta}(\eta,\tau)\to 1,\quad \dfrac{\partial g}{\partial\eta}(\eta,\tau)\to 1,\quad h(\eta,\tau)\to 0,\quad k(\eta,\tau)\to 0\quad \text{as}\quad \eta\to\infty. \end{cases} \tag{30}$$

For the steady flow solution, the stability tests $f(\eta)=f_0(\eta)$, $g(\eta)=g_0(\eta)$, $h(\eta)=h_0(\eta)$, $k(\eta)=k_0(\eta)$, and $\theta(\eta)=\theta_0(\eta)$ accomplish Eqs. (8)–(12). We have[14]

$$\begin{cases} f(\eta,\tau)=f_0(\eta)+\exp(-\gamma\tau)F(\eta,\tau),\quad g(\eta,\tau)=g_0(\eta)+\exp(-\gamma\tau)G(\eta,\tau),\\ h(\eta,\tau)=h_0(\eta)+\exp(-\gamma\tau)H(\eta,\tau),\quad k(\eta,\tau)=k_0(\eta)+\exp(-\gamma\tau)K(\eta,\tau),\\ \theta(\eta,\tau)=\theta_0(\eta)+\exp(-\gamma\tau)\Theta(\eta,\tau). \end{cases} \tag{31}$$

In the above expressions, $\gamma$ indicates the unknown eigenvalue variable, while capital letters $F(\eta,\tau)$, $G(\eta,\tau)$, $H(\eta,\tau)$, $K(\eta,\tau)$, and $\Theta(\eta,\tau)$ are small subject to $f_0(\eta)$, $g_0(\eta)$, $h_0(\eta)$, $k_0(\eta)$, and $\theta_0(\eta)$. The Eigen solutions to Eqs. (25)–(31) give infinite numbers of solutions set dependent on eigenvalues $\gamma_1<\gamma_2<\gamma_3<\gamma_4$[14]; here it is noted that if the smallest $\gamma_1$ is negative, flow is unstable, and if the smallest $\gamma_1$ is positive, flow is stable.

Invoking Eq. (31) into Eqs. (23)–(30), we have the following linearized forms:

$$\Big(\frac{\mu_{\rm nf}}{\mu_{\rm f}}\Big)\Big(\frac{\rho_{\rm f}}{\rho_{\rm nf}}\Big)\frac{\partial^3 F}{\partial\eta^3}+{+}(F+G)f_0''+(f_0+g_0)\frac{\partial^2 F}{\partial\eta^2}-2(1+F_x)f_0'\frac{\partial F}{\partial\eta}$$
$$-\Big(\beta^*\Big(\frac{\mu_{\rm nf}}{\mu_{\rm f}}\Big)\Big(\frac{\rho_{\rm f}}{\rho_{\rm nf}}\Big)-\gamma\Big)\frac{\partial F}{\partial\eta}-\frac{\partial^2 F}{\partial\eta\partial\tau}=0, \tag{32}$$

$$\Big(\frac{\mu_{\rm nf}}{\mu_{\rm f}}\Big)\Big(\frac{\rho_{\rm f}}{\rho_{\rm nf}}\Big)\frac{\partial^3 G}{\partial\eta^3}+(F+G)g_0''+(f_0+g_0)\frac{\partial^2 G}{\partial\eta^2}-2(1+F_y)g_0'\frac{\partial G}{\partial\eta}$$
$$-\Big(\beta^*\Big(\frac{\mu_{\rm nf}}{\mu_{\rm f}}\Big)\Big(\frac{\rho_{\rm f}}{\rho_{\rm nf}}\Big)-\gamma\Big)\frac{\partial G}{\partial\eta}-\frac{\partial^2 G}{\partial\eta\partial\tau}=0, \tag{33}$$

$$\Big(\frac{\mu_{\rm nf}}{\mu_{\rm f}}\Big)\Big(\frac{\rho_{\rm f}}{\rho_{\rm nf}}\Big)\frac{\partial^2 H}{\partial\eta^2}+(f_0+g_0)\frac{\partial H}{\partial\eta}+(F+G)h_0'-\Big(h_0\frac{\partial F}{\partial\eta}+\frac{\partial f_0}{\partial\eta}H\Big)$$
$$-2F_x\Big(\lambda h_0 H+\Big(h_0\frac{\partial F}{\partial\eta}+Hf_0'\Big)\Big)-\Big(\beta^*\Big(\frac{\mu_{\rm nf}}{\mu_{\rm f}}\Big)\Big(\frac{\rho_{\rm f}}{\rho_{\rm nf}}\Big)-\gamma\Big)H-\frac{\partial H}{\partial\tau}=0, \tag{34}$$

$$\Big(\frac{\mu_{\rm nf}}{\mu_{\rm f}}\Big)\Big(\frac{\rho_{\rm f}}{\rho_{\rm nf}}\Big)\frac{\partial^2 K}{\partial\eta^2}+(f_0+g_0)\frac{\partial K}{\partial\eta}+(F+G)k_0'-\Big(k_0\frac{\partial G}{\partial\eta}+g_0'K\Big)$$
$$-2F_y\Big(\lambda_1 k_0 K+\Big(k_0\frac{\partial G}{\partial\eta}+Kg_0'\Big)\Big)-\Big(\beta^*\Big(\frac{\mu_{\rm nf}}{\mu_{\rm f}}\Big)\Big(\frac{\rho_{\rm f}}{\rho_{\rm nf}}\Big)-\gamma\Big)K-\frac{\partial K}{\partial\tau}=0, \tag{35}$$

$$\Big(\frac{1}{Pr}\Big)\Big(\frac{(\rho c_p)_{\rm f}}{(\rho c_p)_{\rm nf}}\Big)\Big(\Big(\frac{k_{\rm nf}}{k_{\rm f}}+R\Big)\Big)\frac{\partial^2\Theta}{\partial\eta^2}+(f_0+g_0)\frac{\partial\Theta}{\partial\eta}+(F+G)\frac{\partial\theta_0}{\partial\eta}$$
$$+\Big(Q\Big(\frac{(\rho c_p)_{\rm f}}{(\rho c_p)_{\rm nf}}\Big)-\gamma\Big)\Theta(\eta,\tau)-\frac{\partial\Theta}{\partial\tau}=0 \tag{36}$$

with

$$\begin{cases} F(0)=0, \quad G(0)=0, \\ \dfrac{\partial}{\partial\eta}F(0)=A\dfrac{\partial^2}{\partial\eta^2}F(0), \quad \dfrac{\partial}{\partial\eta}G(0)=\dfrac{\partial^2}{\partial\eta^2}B(0), \\ H(0)=A\dfrac{\partial}{\partial\eta}H(0), \quad K(0)=B\dfrac{\partial}{\partial\eta}K(0), \\ \dfrac{\partial}{\partial\eta}F(\eta)\to 0, \quad \dfrac{\partial}{\partial\eta}G(\eta)\to 1, \quad H(\eta)\to 0, \quad K(\eta)\to 0 \quad \text{as} \quad \eta\to\infty. \end{cases} \tag{37}$$

Here, we discuss the stability of incompressible and steady state flow by setting $\tau=0$, and thus we have $F=F_0(\eta)$, $G=G_0(\eta)$, $H=H_0(\eta)$, $K=K_0(\eta)$, and $\Theta=\Theta_0(\eta)$ in Eqs. (32)–(36) to recognize the initial growth or decline of solution to Eq. (31). To test the accuracy of our

results, we have the following linear eigenvalue problem:

$$\Big(\frac{\mu_{\rm nf}}{\mu_{\rm f}}\Big)\Big(\frac{\rho_{\rm f}}{\rho_{\rm nf}}\Big)F_0''' + (F_0+G_0)f_0'' + (f_0+g_0)F_0'' - 2(1+F_x)f_0'F_0'$$
$$-\Big(\beta^*\Big(\frac{\mu_{\rm nf}}{\mu_{\rm f}}\Big)\Big(\frac{\rho_{\rm f}}{\rho_{\rm nf}}\Big)-\gamma\Big)F_0' = 0, \tag{38}$$

$$\Big(\frac{\mu_{\rm nf}}{\mu_{\rm f}}\Big)\Big(\frac{\rho_{\rm f}}{\rho_{\rm nf}}\Big)G_0''' + (F_0+G_0)g_0'' + (f_0+g_0)G_0'' - 2(1+F_y)g_0'G_0'$$
$$-\Big(\beta^*\Big(\frac{\mu_{\rm nf}}{\mu_{\rm f}}\Big)\Big(\frac{\rho_{\rm f}}{\rho_{\rm nf}}\Big)-\gamma\Big)G_0' = 0, \tag{39}$$

$$\Big(\frac{\mu_{\rm nf}}{\mu_{\rm f}}\Big)\Big(\frac{\rho_{\rm f}}{\rho_{\rm nf}}\Big)H_0'' + (f_0+g_0)H_0' + (F_0+G_0)h_0' - \Big(h_0F_0' + \frac{\partial f_0}{\partial\eta}H_0\Big)$$
$$-2F_x\Big(\lambda h_0H_0 + \Big(h_0F_0' + H_0f_0'\Big)\Big) - \Big(\beta^*\Big(\frac{\mu_{\rm nf}}{\mu_{\rm f}}\Big)\Big(\frac{\rho_{\rm f}}{\rho_{\rm nf}}\Big)-\gamma\Big)H_0 = 0, \tag{40}$$

$$\Big(\frac{\mu_{\rm nf}}{\mu_{\rm f}}\Big)\Big(\frac{\rho_{\rm f}}{\rho_{\rm nf}}\Big)K_0''' + (f_0+g_0)\frac{\partial K}{\partial\eta} + (F_0+G_0)k_0' - \Big(k_0G_0' + g_0'K_0\Big)$$
$$-2F_y\Big(\lambda_1k_0K_0 + \Big(k_0G_0' + K_0g_0'\Big)\Big) - \Big(\beta^*\Big(\frac{\mu_{\rm nf}}{\mu_{\rm f}}\Big)\Big(\frac{\rho_{\rm f}}{\rho_{\rm nf}}\Big)-\gamma\Big)K_0 = 0, \tag{41}$$

$$\Big(\frac{1}{Pr}\Big)\Big(\frac{(\rho c_p)_{\rm f}}{(\rho c_p)_{\rm nf}}\Big)\Big(\Big(\frac{k_{\rm nf}}{k_{\rm f}}+R\Big)\Big)\Theta_0'' + (f_0+g_0)\Theta_0' + (F_0+G_0)\frac{\partial\theta_0}{\partial\eta}$$
$$+\Big(Q\Big(\frac{(\rho c_p)_{\rm f}}{(\rho c_p)_{\rm nf}}\Big)-\gamma\Big)\Theta_0(\eta,\,\tau) = 0 \tag{42}$$

with

$$\begin{cases} F_0(0)=0, \quad F_0'(0)=AF_0''(0), \quad G_0(0)=0, \quad G_0'(0)=BG_0''(0), \\ H_0(0)=AH_0'(0), \quad K_0(0)=BK_0'(0), \\ F_0'(\eta)\to 0, \quad G_0'(\eta)\to 1, \quad H_0(\eta)\to 0, \quad K_0(\eta)\to 0 \quad \text{as} \quad \eta\to\infty. \end{cases} \tag{43}$$

For specific ranges of $\xi$, $s$, $A$, and $B$, the stability investigation of the corresponding incompressible and steady flow solution $f_0(\eta)$, $g_0(\eta)$, $h_0(\eta)$, $k_0(\eta)$, and $\theta_0(\eta)$ is determined subject to smallest $\gamma_1$. The range of possible $\gamma_1$ and the range of possible eigenvalues can be obtained by fixing $F_0(\eta)$, $G_0(\eta)$, $H_0(\eta)$, $K_0(\eta)$, and $\Theta_0(\eta)$. Therefore, we have $G_0'(\eta)\to 1$ as $\eta\to\infty$, and for a fixed range of $\gamma$, the system of expressions (38)–(42) with new type of boundary constraint $G_0''=1$ is tackled.

## 4 Results and discussion

Here, the 3D steady and incompressible laminar Homann stagnation point nanofluid flow over a porous moving surface is addressed. The disturbance in porous medium has been characterized by Darcy-Forchheimer relation. The slip for viscous fluid is considered. The energy equation is organized in view of radiative heat flux and heat generation absorption effects which plays an important role in the heat transfer rate. Table 1 highlights the transport characteristics of nanofluids. The governing flow expressions are first altered into first-order ordinary ones and then solved numerically by the shooting method (bvp4c). Dual solutions are obtained. Therefore, the computational outcomes are obtained for the nonlinear ordianry ones and Eqs. (8)–(11) subject to boundary constraints (12) utilizing shooting method (bvp4c). To

validate the accuracy of the obtained outcomes, $f''(0)$ and $g'(0)$ are compared with the results of Wang[21] in Table 2, and good analysis with them is found. All the nonlinear ordinary ones are coupled, and thus tackled simultaneously. Here, we take the value of $\eta_\infty$ between 4 and 10.

**Table 2** Comparison and relative error of $f''(0)$ and $g'(0)$ with well-organized results of Wang[21] subject to $A = B$ in limiting case

| $A$ | $B$ | Present result | Wang[21] | Relative error |
|---|---|---|---|---|
| 0 | $f''(0)$ | 1.311 938 | 1.311 938 | 0.000 0 |
| | $g'(0)$ | –0.938 73 | –0.938 73 | 0.000 0 |
| 0.5 | $f''(0)$ | 0.866 88 | 0.866 88 | 0.000 0 |
| | $g'(0)$ | –0.749 87 | –0.749 87 | 0.000 0 |
| 1.0 | $f''(0)$ | 0.617 30 | 0.617 30 | 0.000 0 |
| | $g'(0)$ | –0.564 53 | –0.564 53 | 0.000 0 |

Salient characteristics of the surface drag forces, i.e., $f''(0)$ subject to rising values of porosity parameter and Darcy-Forchheimer number in the $x$-direction and fixing $\xi = 1$, are scrutinized in Table 3. As anticipated, the magnitude of drag force declines versus these variables. Various variations of Nusselt number, i.e., $\theta'(0)$ versus rising estimation of thermal radiation and heat generation/absorption, are illustrated in Table 4. Here, it is noticed from Table 4, that both the UBS and the LBS decrease versus generation/absorption parameter while for radiation parameter both the UBS and the LBS show contrast impact. The UBS decreases versus radiation parameter while the LBS increases via this variable. Figure 1 is captured for the physical interpretation of schematic flow analysis. Figures 2 and 3 are organized to check how the velocity components affects versus higher values of magnetic parameter ($M = 0.1$, 0.2, 0.3). As anticipated, both solutions are declined via rising magnetic parameter. Through stability examinations, the UBS is more reliable and stable than the lower branch solution. Physically, the curves of velocity components declines due to Lorentz force, which is resistive force to the motion of the fluid particles. That is why velocity declines. Figures 4 and 5 are captured to examine the behavior of porosity variable ($\beta^* = 0.00$, 0.05, 0.10) on the velocity components i.e., $f'(\eta)$ and $g'(\eta)$. Again, both solutions, i.e., the UBS and the LBS are decreased against larger porosity parameter. In physical point of view, larger porosity variable generates more resistive force to the motion of the material particles and as a results the velocity of the material particles are disturbed greatly by larger porosity parameter. Effects of Darcy-Forchheimer number ($F_x = 0.00$, 0.05, 0.10) on the velocity components are developed in Figs. 6 and 7. Here, it is noticed from Fig. 6 that both the UBS and the LBS predict contrast impact against larger Forchheimer number. The UBS diminishes while the LBS boosts via rising Darcy-Forchheimer number. Also, it is remarked that the layer shows dual impact versus Darcy-Forchheimer number. But, in Fig. 7, both the UBS and the LBS decay versus larger Darcy-Forchheimer number. Furthermore, axial velocity fields, i.e., $h(\eta)$ and $k(\eta)$ versus second-order slip parameter and moving variables $\xi = 0.5$ and $\xi = -0.5$ when $s = 0.5$ and $A = 0.1$, are highlighted in Figs. 8 and 9. Clearly, both Figs. 8 and 9 depict that the increase of second-order slip parameter causes the decline in boundary layer thinness, and therefore, boosts the velocity gradient. Figures 10 and 11 describe the thermal fields versus higher estimation of radiation parameter ($R = 0.1$, 0.3, 0.5) and heat generation/absorption parameter ($Q = 0.3$, 0.6, 0.9). For rising estimations of radiative parameter and heat generation parameter, the thermal field and associated layer are gradually boosts against these parameters. The mean absorption coefficient decays versus larger radiation parameter, and as a result the temperature field increases. The same influence on the thermal field is observed in Fig. 11. As anticipated, both the thermal field and layer thickness decay rising radiation and heat generation parameters.

**Table 3** Results of skin friction coefficient for both the UBS and the LBS subject to $\beta^*$ and $F_x$

| $\beta^*$ | $F_x$ | UBS | LBS |
|---|---|---|---|
| 0.0 | 0.05 | 1.265 7 | –0.194 4 |
| 0.05 | | 1.237 5 | –0.110 1 |
| 0.1 | | 1.210 2 | –0.030 9 |
| 0.05 | 0.0 | 1.258 5 | –0.104 8 |
| | 0.05 | 1.237 5 | –0.110 1 |
| | 0.1 | 1.217 7 | –0.115 6 |

**Table 4** Results of Nusselt number for both the UBS and the LBS subject to $Q$ and $R$

| $Q$ | $R$ | UBS | LBS |
|---|---|---|---|
| 0.01 | 0.5 | 1.029 4 | 0.163 3 |
| 0.02 | | 1.023 5 | 0.129 1 |
| 0.03 | | 1.017 5 | 0.092 6 |
| 0.01 | 0.5 | 1.029 4 | 0.163 3 |
| | 1.0 | 0.979 0 | 0.170 1 |
| | 1.5 | 0.935 9 | 0.175 1 |

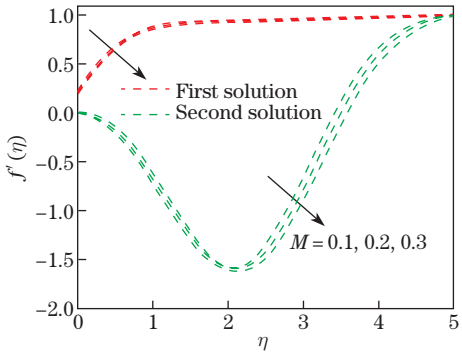


**Fig. 2** Velocity behavior $f'(\eta)$ versus $M$ (color online)

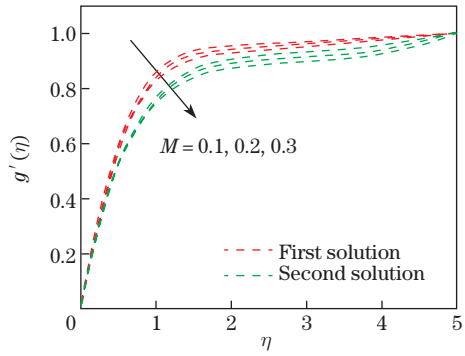


**Fig. 3** Velocity behavior $g'(\eta)$ versus $M$ (color online)

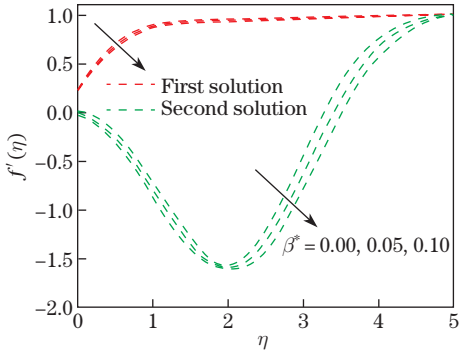


**Fig. 4** Velocity behavior $f'(\eta)$ versus $\beta^*$ (color online)

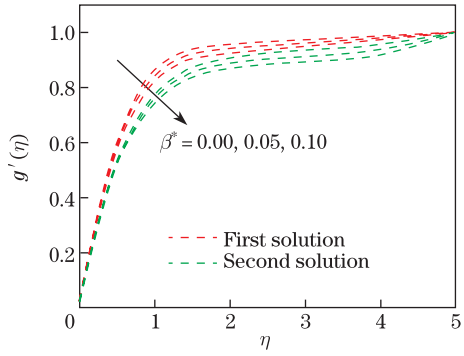


**Fig. 5** Velocity behavior $g'(\eta)$ versus $\beta^*$ (color online)

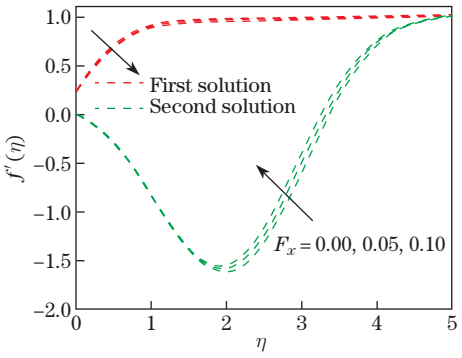


**Fig. 6** Velocity behavior $f'(\eta)$ versus $F_x$ (color online)

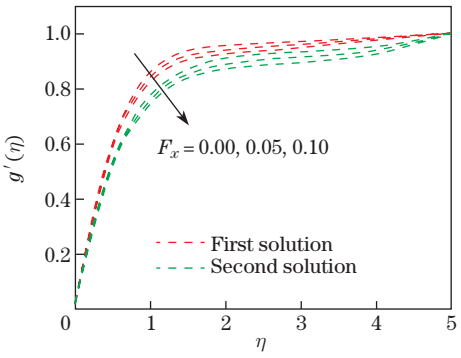


**Fig. 7** Velocity behavior $g'(\eta)$ versus $F_x$ (color online)

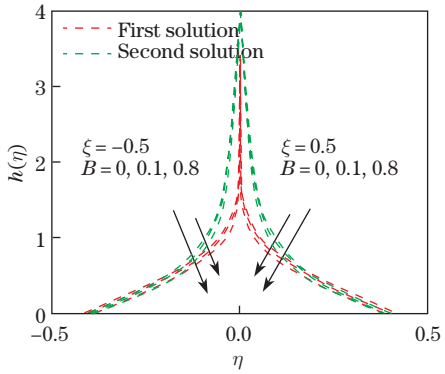


**Fig. 8** Axial velocity $h(\eta)$ versus $B$ (color online)

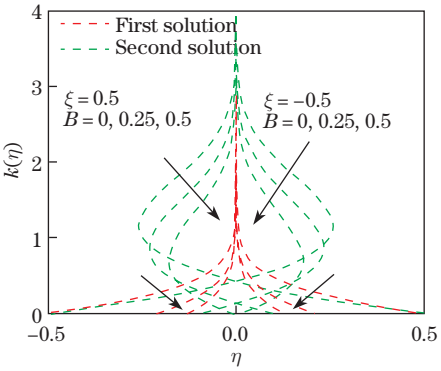


**Fig. 9** Axial velocity $k(\eta)$ versus $B$ (color online)

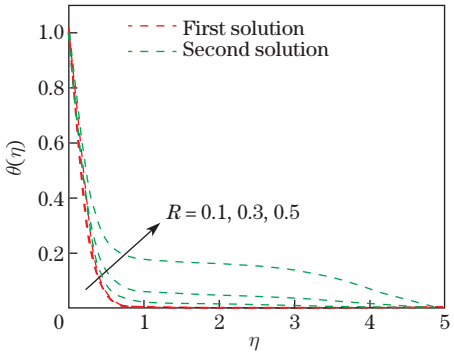


**Fig. 10** Temperature field $\theta(\eta)$ versus $R$ (color online)

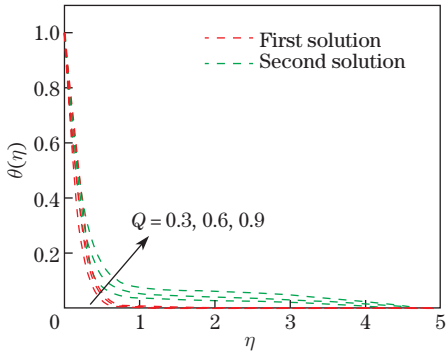


**Fig. 11** Temperature field $\theta(\eta)$ versus $Q$ (color online)

## 5 Conclusions

In this research, the 3D incompressible, steady, and saturated flow of viscous fluid by a moving surface is addressed in the presence of Darcy-Forchheimer porous relation, thermal

radiation, first- and second-order velocity slips, and heat generation/absorption effects. The governing flow expressions are first altered into first-order ordinary ones and then numerically solved versus the shooting method (bvp4c). Some valuable and important results are summarized as follows.

(i) The UBS is more reliable and stable than the LBS.

(ii) The velocity field declines for both solutions, i.e., the UBS and the LBS versus the porosity parameter, the Darcy-Forchheimer number, and the magnetic parameter.

(iii) The temperature distribution is more higher for both the UBS and the LBS against the radiation parameter and the heat generation/absorption parameter.

(iv) The skin friction decays more earlier against the larger Darcy-Forchheimer number and the porosity parameter.

(v) The heat transfer rate (Nusselt number) boosts against the higher estimations of radiation for the LBS case and declines against the heat generation/absorption parameter for the UBS case.

## References


[1] FANG, T., ZHANG, J., and YAO, S. A new family of unsteady boundary layers over a stretching surface. *Applied Mathematics and Computation*, **217**, 3747–3755 (2010)

[2] KHAN, M. I., WAQAS, M., HAYAT, T., and ALSAEDI, A. A comparative study of Casson fluid with homogeneous-heterogeneous reactions. *Journal of Colloid and Interface Science*, **498**, 85–90 (2017)

[3] SAHOO, B. and SHEVCHUK, I. V. Heat transfer due to revolving flow of Reiner-Rivlin fluid over a stretchable surface. *Thermal Science and Engineering Progress*, **10**, 327–336 (2019)

[4] KHAN, M., AHMAD, J., and AHMAD, L. Chemically reactive and radiative von Kármán swirling flow due to a rotating disk. *Applied Mathematics and Mechanics* (*English Edition*), **39**(9), 1295–1310 (2018) https://doi.org/10.1007/s10483-018-2368-9

[5] MUHAMMAD, R., KHAN, M. I., KHAN, N. B., and JAMEEL, M. Magnetohydrodynamics (MHD) radiated nanomaterial viscous material flow by a curved surface with second order slip and entropy generation. *Computer Methods and Programs in Biomedicine*, **189**, 105294 (2020)

[6] SAKIADIS, B. C. Boundary layer behavior on continuous solid surfaces: I. boundary layer equations for two dimensional and axisymmetric flow. *AIChE Journal*, **7**, 26–28 (1961)

[7] CRANE, L. J. Flow past a stretching plate. *Journal of Applied Mathematics and Physics* (*ZAMP*), **21**, 645–647 (1970)

[8] RASHIDI, M. M., ALI, M., ROSTAMI, B., ROSTAMI, P., and XIE, G. N. Heat and mass transfer for MHD viscoelastic fluid flow over a vertical stretching sheet with considering soret and Dufour effects. *Mathematical Problems in Engineering*, **2015**, 861065 (2015)

[9] WAQAS, H., IMRAN, M., KHAN, S. U., SHEHZAD, S. A., and MERAJ, M. A. Slip flow of Maxwell viscoelasticity-based micropolar nanoparticles with porous medium: a numerical study. *Applied Mathematics and Mechanics* (*English Edition*), **40**(9), 1255–1268 (2019) https://doi.org/10.1007/s10483-019-2518-9

[10] MUHAMMAD, R., KHAN, M. I., JAMEEL, M., and KHAN, N. B. Fully developed Darcy-Forchheimer mixed convective flow over a curved surface with activation energy and entropy generation. *Computer Methods and Programs in Biomedicine*, **188**, 105298 (2020)

[11] SUN, X., WANG, S., and ZHAO, M. Numerical solution of oscillatory flow of Maxwell fluid in a rectangular straight duct. *Applied Mathematics and Mechanics* (*English Edition*), **40**(11), 1647–1656 (2019) https://doi.org/10.1007/s10483-019-2535-6

[12] SCHLICHTING, H. *Boundary Layer Theory*, 7th Edition, McGraw-Hill, New York (1960)

[13] CHARI, K. and RAJAGOPALAN, R. Deposition of colloidal particles in stagnation-point flow. *Journal of the Chemical Society, Faraday Transactions*, **81**, 1345–1366 (1985)

[14] HAFIDZUDDIN, E. H., NAZAR, R., ARIFIN, N. M., and POP, I. Effects of anisotropic slip on three-dimensional stagnation-point flow past a permeable moving surface. *European Journal of Mechanics-B/Fluids*, **65**, 515–521 (2017)

[15] BÉG, O. A., BAKIER, A. Y., PRASAD, V. R., ZUECO, J., and GHOSH, S. K. Nonsimilar, laminar, steady, electrically-conducting forced convection liquid metal boundary layer flow with induced magnetic field effects. *International Journal of Thermal Sciences*, **48**, 1596–1606 (2019)

[16] SHAH, F., KHAN, M. I., HAYAT, T., MOMANI, S., and KHAN, M. I. Cattaneo-Christov heat flux (CC model) in mixed convective stagnation point flow towards a Riga plate. *Computer Methods and Programs in Biomedicine*, **196**, 105564 (2020)

[17] AL-BALUSHI, L. M., RAHMAN, M. M., and POP, I. Three-dimensional axisymmetric stagnation-point flow and heat transfer in a nanofluid with anisotropic slip over a striated surface in the presence of various thermal conditions and nanoparticle volume fractions. *Thermal Science and Engineering Progress*, **2**, 26–42 (2017)

[18] KHAN, M. I., ALZAHRANI, F., HOBINY, A., and ALI, Z. Modeling of Cattaneo-Christov double diffusions (CCDD) in Williamson nanomaterial slip flow subject to porous medium. *Journal of Materials Research and Technology*, **9**, 6172–6177 (2020)

[19] MAHAPATRA, T. R. and SIDUI, S. Non-axisymmetric Homann stagnation-point flow of a viscoelastic fluid towards a fixed plate. *European Journal of Mechanics-B/Fluids*, **79**, 38–43 (2020)

[20] KHAN, M., EL SHAFEY, A. M., SALAHUDDIN, T., and KHAN, F. Chemically Homann stagnation point flow of Carreau fluid. *Physica A: Statistical Mechanics and Its Applications*, **551**, 124066 (2020)

[21] WANG, C. Stagnation slip flow and heat transfer on a moving plate. *Chemical Engineering Science,* **61**, 7668–7672 (2006)

[22] WEIDMAN, P., KUBITSCHEK, D., and DAVIS, A. The effect of transpiration on self-similar boundary layer flow over moving surfaces. *International Journal of Engineering Sciences*, **44**, 730–737 (2006)